AIAA 98–2851

A Passive Earth-Entry Capsule for Mars Sample Return

R. A. Mitcheltree , S. Kellas, J. T. Dorsey, P. N. Desai, C. J. Martin
NASA Langley Research Center, Hampton, Virginia

7th AIAA/ASME Joint Thermophysics and Heat Transfer Conference
June 15–18, 1998/Albuquerque, NM

A Passive Earth-Entry Capsule for Mars Sample Return

R. A. Mitcheltree *, S. Kellas†, J. T. Dorsey‡, P. N. Desai§, C. J. Martin¶
NASA Langley Research Center, Hampton, Virginia

A combination of aerodynamic analysis and testing, aerothermodynamic analysis, structural analysis and testing, impact analysis and testing, thermal analysis, ground characterization tests, configuration packaging, and trajectory simulation are employed to determine the feasibility of an entirely passive Earth entry capsule for the Mars Sample Return mission. The design circumvents the potential failure modes of a parachute terminal descent system by replacing that system with passive energy absorbing material to cushion the Mars samples during ground impact. The suggested design utilizes a spherically blunted 45 degree half-angle forebody with an ablative heatshield. The primary structure is a spherical composite sandwich enclosing carbon foam energy absorbing material. Though no demonstration test of the entire system is included, results of the testing and analysis presented indicate that the design is a viable option for the Mars Sample Return Mission.

Introduction

The Mars Sample Return (MSR) mission will return selected samples from Mars to Earth. The final phase of the mission requires an Earth entry, descent, and landing capsule. Since the MSR mission must be accomplished within stringent cost and mass restrictions, the Earth-entry subsystem must be both simple and low mass. In addition, the National Research Council's Task Group on Issues in Sample Return[1] has determined that the potential for terrestrial contamination from Mars samples, while minute, is not zero. The sample return capsule must, therefore, assure containment of the samples. To assure containment, the capsule must either 1) include sufficient redundancy to each critical subsystem or 2) eliminate the need for that subsystem. Eliminating subsystems rather than adding redundant systems is essential for MSR because of the mass restrictions on the capsule. This paper describes a elegantly simple option for the Mars Sample Return Earth entry capsule.

The desire to obtain extraterrestrial samples for Earth-based analysis has spawned several upcoming sample return missions with destinations *besides* Mars. The fourth discovery class mission, Stardust[2,3] (launch Feb. 1999), plans to return cometary coma samples and interstellar dust in 2006. The Muses CN mission is scheduled for a 2002 launch and will attempt to return asteroid samples in 2006. The fifth discovery class mission, Genesis, promises to collect samples of the solar wind for return in 2003. All three of these missions utilize direct entry capsules with parachute terminal descent. The New Millennium Project Deep Space 4 mission, Champollion, plans to return comet nucleus samples in 2010.

Sample return missions for Mars have been studied periodically for the past 30 years[4–6]. The Earth entry phase envisioned by previous studies involved either 1) an orbit insertion at Earth with Space Shuttle or Space Station rendezvous for recovering the samples or 2) direct entry with an Apollo-style entry vehicle utilizing parachutes, air-snatch, and/or water recovery. The first scenario is prohibitively expensive, the second relies on fallible entry events. All of the previous studies involved entry vehicles with masses significantly larger than the current 30 kg allotment for the 2005 opportunity.

Direct entry of a passive capsule which does not include a parachute terminal descent system but relies solely on aerodynamics for deceleration and attitude control may represent the lowest mass, least expensive, and most robust entry scenario. In such a design, the samples are packaged in a hardened container and surrounded by sufficient energy-absorbing material to assure containment during the resulting ground impact. The objective of this work is to examine one candidate Earth-entry capsule within this scenario to explore the feasibility of the approach.

The present work utilizes high-fidelity, multidisciplinary analysis in the conceptual design phase. A combination of static and dynamic aerodynamic evaluations are supplied through new and existing wind tunnel measurements augmented by computational fluid

*Aerospace Engineer, Aerothermodynamics Branch, Aero- and Gas Dynamics Division, NASA Langley Research Center, Senior Member AIAA.

†Principal Engineer, Lockheed Martin Engineering and Sciences Co., Hampton Va.

‡Aerospace Engineer, Thermal Structures Branch, Structures Division, NASA Langley Research Center, Senior Member AIAA.

§Aerospace Engineer, Vehicle Analysis Branch, Space Systems and Concepts Division, NASA Langley Research Center, Senior Member AIAA.

¶Aerospace Engineer, Thermal Structures Branch, Structures Division, NASA Langley Research Center.

dynamics (CFD) predictions to cover the entire entry speed range (hypersonic through subsonic). Aerothermal heating predictions, heatshield design, and thermal analysis of the entry and impact are included. Impact energy absorption is examined through crush testing and drop tests. Structural design utilizes finite element analysis and impact tests. Ground characterization test data from the Utah Test and Targeting Range (UTTR) is included. Solid modeling of the design is used to address packaging issues and estimate the mass properties of the vehicle. Detailed trajectory simulations and dispersion analyses are performed using the three-degree-of-freedom Program to Optimize Simulated Trajectories (POST)[7]. Carrier vehicle integration and canister injection issues are also mentioned.

After a brief description of the sample return capsule's requirements, the major design drivers - as currently understood - are identified. Next, a non-conventional approach to the design based on spherical shapes which have no directional preference during entry and impact is discussed. The remainder of the paper describes analysis performed on one possible directional design for the capsule. The combination of these analyses point to the feasibility of this design for Mars Sample Return. This work also has direct application to future sample return missions.

System Requirements and Design Drivers

The primary requirement on the Earth-entry capsule is to assure containment of the Mars samples during the intense Earth entry, descent, and impact phase of the mission. This planetary protection concern led to the consideration of a parachute-less entry since exclusion of that descent subsystem eliminates a major vehicle failure mode and reduces mass and complexity of the vehicle. The design must also provide for easy sample recovery which requires ground recovery beacons and discourages a water landing. The overall vehicle mass must be less than 30 kg with a maximum dimension of 1.0 m.

As many as 90 core samples of Mars rock and regolith totaling 300 grams will be hermetically sealed within a canister on the surface of Mars. This hardened canister, whose external surfaces will be kept clean while on Mars, must be transferred to the Earth-entry capsule in Mars orbit. (In this paper, the term *canister* refers to the hardened container of the samples, while the term *capsule* refers to the entire entry vehicle.) At Earth return, the capsule is spun up and released from the Earth cruise stage for entry. After traversing hypersonic, supersonic, transonic and subsonic speed regimes, the capsule will impact the ground traveling at subsonic, terminal velocity. During impact, the system must limit mechanical loads on the sample canister below prescribed limits. In addition, the temperatures of the samples must be maintained below 370 K. The shape, size, mass, and mechanical strength of the sample canister are major drivers in the design of the Earth-entry system. For this study, the canister is assumed to be a sphere of 0.2 m diameter with mass of 2.7 kg which is designed to handle mechanical loads in the range of 200 to 300 g's.

The capsule's relative entry velocity at 125 km altitude is in excess of 11 km/s, depending on the Earth return trajectory. This high-energy entry drives the design to a blunt aeroshell with an ablating heat shield to protect the vehicle from the intense heating environment expected in the first 60 seconds of the entry. Aerodynamic decelerations between 40 and 80 Earth g's occur during this portion of the entry. After 100 seconds, the capsule has decelerated to around Mach 1.0 and descended to 30-35 km altitude. For the remaining 500 seconds of the entry the capsule descends at subsonic speeds. Blunt aeroshell shapes which can survive the intense heating of the hypersonic heatpulse, often suffer aerodynamic stability problems in the transonic and subsonic regimes. The conflicting requirements of minimizing heating while maximizing subsonic aerodynamic stability is a major design trade in selecting the aeroshell shape.

Surface winds are also a major design driver. The capsule must be designed to accommodate 25 MPH sustained surface winds at impact. Winds increase impact velocity and introduce large surface incidence angles.

Omni-Directional Designs

Impact loads on the sample-containing canister can be reduced by packaging that canister behind a thick layer of energy absorbing material. Such an arrangement places the canister as far as possible from the impacting surface. Simultaneously, for concepts which are intended to always fly with a particular surface (i.e. the nose) forward, subsonic aerodynamic stability during the terminal descent phase requires the center-of-gravity (c.g.) to be as close as possible to the nose. These conflicting requirements lead to consideration of omni-directional designs. An omni-directional design is one which has no directional preference during entry or impact.

The simplest omni-directional design is a sphere with c.g. at the geometric center of the body. Figure 1 shows a concept in which the sample canister is embedded within low-mass energy-absorbing foam which is then encapsulated within a thin shell structure and Phenolic Impregnated Carbon Ablator (PICA-15) heat shield. To assess the feasibility of this concept, an optimistic set of design assumptions is made. The subsonic drag coefficient (C_D) of a sphere can be as high as 0.5 for laminar flow conditions[8]. For the present conditions (flight Reynolds numbers greater than 10^6), the

flow will be turbulent, and C_D can be as low as 0.1[8]. To be optimistic, C_D is set to 0.2. Engineering level tools are used to compute the necessary stagnation point heat shield thickness for each size/mass combination. If the sphere is tumbling at 10 rpm or greater during entry, the heat load at a given point is decreased by two thirds. This decreases the required heat shield thickness by one third. Thus, this "rotisserie" relieving effect is assumed, and the heat shield thickness is specified as two thirds of that for an equivalent stagnation point. It is further assumed, without verification, that a 0.001 m composite shell structure is sufficient to remain essentially undeformed at impact. Even with these optimistic assumptions, the figure reveals that a 25 kg capsule still results in an impact which imparts 1000-1200 g's on the canister as it decelerates over the available stroke distance. The capsule is assumed to hit a rigid surface.

The primary difficulty with a spherical entry capsule is the low subsonic drag coefficient which produces high ground-impact velocities. The drag coefficient for a sphere decreases in turbulent conditions because the flow stays attached to the surface beyond the maximum diameter location. In an attempt to force the separation and increase the subsonic drag coefficient, several modified sphere concepts were considered. Two of these are presented in Fig. 2. Many other concepts are possible but most, including those shown in the figure, introduce heating concentrations in regions where the local radius of curvature is small. Drop tests and spin-tunnel[9] tests were performed on scale models of these configurations in an attempt to determine their drag coefficients. The Reynolds numbers of these tests were too low to produce turbulent flow fields, and direct measurement of the drag coefficient was difficult. By modifying a sphere's surface to force flow separation at the maximum diameter location, the highest subsonic drag coefficient that could be envisioned without introducing insurmountable heating problems was the value for a laminar sphere: 0.5.

Figure 3 repeats the analysis shown in Fig. 1 with C_D equal to 0.5. In addition to the optimism included in Fig. 1, the calculations to produce Fig. 3 assume whatever modification is necessary to increase the drag does not increase the mass or decrease the stroke of an equivalent diameter sphere. The expected decelerations for a hard ground impact of a 25 kg capsule are decreased to 400-600 g's. To decrease decelerations below 300 g's requires a capsule diameter larger than 1.3 m with associated mass over 100 kg.

A spherical entry capsule has a very low subsonic drag coefficient. In addition, the requirement to carry heat shield over the entire outer surface of the shape results in large heat shield mass. This combination results in large subsonic ballistic coefficients and their associated large impact energies. While it may be possible to devise a modified spherical shape with increased subsonic drag, obtaining a C_D larger than 0.5 would be difficult.

Heat shield seals and penetrations to accomplish attachment to the orbiter, insertion of the canister, and electrical connections also present a problem for omni-directional designs since those locations may encounter maximum stagnation point heating during the entry. In addition, the placement of canister-transfer mechanisms and ground-recovery beacons is difficult within a design which may impact at any orientation.

The feasibility of maintaining sample canister loads below 200-300 g's using an omni-directional design for a parachute-less Earth entry system is questionable unless very soft ground or water is impacted.

Hybrid Directional Design

An ideal design for the Earth-entry subsystem would be one that combines the large range of impact-attitude capabilities of an omni-directional design with the forebody-only heatshield and high subsonic drag benefits of a directional design. Such a design would be directional during flight yet nearly omni-directional at impact. Figure 4 presents a schematic of such a "hybrid" directional design based on a 1.0 m diameter 45 degree half-angle forebody. The sample canister is packaged within energy absorbing material. The primary structure is a stiff, spherical, composite-sandwich shell. The heatshield is 0.0381 m thick PICA-15.

Canister transfer access, attachment hard points, and electrical connections are "hidden" in the lower heating region of the afterbody. The canister is positioned such that a large range of primary impact angles can be handled as well as the lower energy impacts resulting from bounces. It is beyond the scope of this paper to discuss all of the trades which were examined in evolving this design. The remainder of the paper examines each element of this design to illustrate its feasibility.

Energy Absorbing Material

At impact, a complex interaction of events occurs whose sum is the removal of the impact kinetic energy. Energy is absorbed by the ground, by the heatshield, by deformation and failure of the capsule structures, and by crush of the energy absorbing material. The goal of the design is to limit mechanical loads on the sample canister at impact. This section focuses on selection and testing of the energy absorbing material to meet that goal.

The design of the canister will dictate its maximum allowable deceleration load. The most efficient deceleration profile for the canister during ground impact is one which is relatively flat at or just below that maximum limit. This constant deceleration represents an ideal crush response.

There are two possibilities for crush energy management in the design of the capsule to achieve an

ideal crush response. In the first, the outer surface of the aeroshell (heatshield, structure, and energy absorbing material) crushes inward towards the canister. This scenario places no particular requirements on the capsule structure or the shape of the canister. Obtaining an ideal crush response, however, requires precise knowledge of the ground's impact characteristics, the structure's strength during failure, and requires a tailored strength gradient be built into the energy absorbing material. The second possibility is to design the capsule with a rigid outer shell structure such that, at impact, the shell deformation is limited. The canister decelerates as it travels into the energy absorbing material. This second approach has the disadvantages that 1) the canister shape becomes important with preference towards a spherical shape to present a constant projected area to the energy absorbing material despite attitude at impact, and 2) the structural mass is increased. Obtaining an ideal crush response with this approach, however, is simplified. In addition, the stiff structure can be used to support attachments to the cruise stage. The second approach – a stiff-outer-structure approach – is taken.

The crushing strength of the energy absorbing material required to limit loads on the canister is independent of the impact velocity. For example, if the sample canister is a 0.2 m diameter sphere of mass 2.7 kg, the desired crushing strength of the material is 24.5 psi to limit accelerations to 200 g's. The required crush stroke depends on the impact velocity and the g-level limit and will be discussed later.

In addition to a tailorable compressive strength, the material selected for energy absorption must be a good thermal insulator and maintain its strength at elevated temperatures. It must be nearly isotropic, and be able to survive launch environment acoustic loads. It must be thermally stable, and must be either open cell for venting in vacuum or, if closed cell, must possess sufficient strength to avoid cell rupture in vacuum. Finally, its crush strength must be strain-rate insensitive over a large range to achieve an ideal crush response.

Honeycombs of paper, metal, polymer, and fiber reinforced plastics were considered as well as rigid, and semi-rigid foams of carbon, metal, ceramic, and plastic. The honeycombs are anisotropic and poor thermal insulators. Plastic foams have a small operating temperature range, and ceramics are heavy.

Reticulated vitreous carbon foam is an open cell material with exceptional chemical inertness, high temperature strength, and low thermal conductivity. The material has the additional benefit that its brittle failure mode is very localized and predictable. Over 180 static tests and 75 dynamic tests were performed on carbon foam samples from three manufacturers. Some representative results are included here to 1) illustrate its suitability as an energy absorber, and 2) estimate the density of the material required for this application.

Carbon foam is currently manufactured at different densities and compressive strengths, most of which exceed the required strengths for this application. Static and dynamic crush response of one form of the material is shown in Fig. 5. The static tests reveal a nearly constant strength for over 90 percent strain. (Crush stroke was limited in the dynamic tests by the available kinetic energy at impact.) To illustrate that the material strength can be "tailored" to a desired value, a planar structure was created by removing hexagonal cores from 2.5 cm thick slab of the material. The slabs were then stacked with a 0.002 m carbon foam sheet between layers to create a honeycomb-like solid whose density was 16 kg/m^3. The resulting static strength of a typical sample was measured to be between 10 and 15 psi. This "machined" approach to tailoring the strength introduces anisotropies into the material. Different approaches to tailor the strength of the material are possible which minimize the introduction of anisotropies.

Figure 5 reveals the compressive strength of carbon foam appears to be rate sensitive. A factor of 2.7 increase in compressive strength was measured when the crush rate was increased from 0.0004 m/s to 1.6 m/s. (Impact speeds are expected to be around 30 m/s.) Dynamic tests in vacuum revealed that the apparent rate sensitivity is not a viscous effect. The increase in strength is believed to be the result of the interaction between the smooth indentor and the rough foam surface. If a suitable coating is deposited on the foam surface which causes more of the foam to become engaged during contact, an increase in static strength, comparable to that observed in the dynamic tests, is realized. This surface coating effect is presented in Fig. 6 and indicates that the rate sensitivity could be reduced by an appropriate surface coating.

Acoustic vibration tests at 140 db (0-500 HZ) for 1.5 min revealed the material can survive severe acoustic launch loads.

Increasing the carbon foam temperature from 300 K to 425 K and 525 K reveals only 20 and 28.6 percent reductions in strength respectively. (The temperature of the foam at impact should be around 300 K with a thin layer near the stagnation point approaching 400 K.)

By combining the information from all of the tests performed, an estimate of the relationship between density and strength for the material can be produced. It appears that 1) carbon foam is a suitable candidate for the energy absorbing material, 2) its strength can be tailored to desired values, and 3) an energy absorber whose strength is "tailored" to 24.5 psi would have density at or below 24 kg/m^3 and provide 90 percent usable stroke.

Ground Characterization Tests

Selecting a crush-energy-management approach based on a rigid outer shell structure removed the influence of the ground's impact characteristics on the design of the energy absorbing material. The need to understand the ground, however, remains necessary to determine the loads to design the structure.

The location for the impact is not determined. One possibility is the dry lake bed at UTTR. Dynamic impact tests were performed at UTTR using a 0.21 m diameter hemispherical penetrometer. The penetrometer contained a 500-g range, 3-axis accelerometer and was dropped from heights of 1.5, 3.0, and 5.9 m. The mass of the indentor, m, could be set at 6.16 or 8.71 kg. Accelerometer data was acquired at a rate of 3200 samples per second.

High winds and inclement weather during the tests limited the quantity and quality of the data collected. Table 1 presents a summary of the impact tests performed.

Table 1. Ground Impact Tests and Results.

Mass, kg	V_i, m/s	a_{max}, g	y_{max}, in
6.16	5.4	52.1	1.4
6.16	5.4	48.9	2.0
6.16	5.4	78.4	1.0
6.16	5.4	81.5	0.8
6.16	7.7	99.2	1.7
6.16	7.7	108.4	1.4
6.16	10.7	124.8	1.8
6.16	10.7	91.8	3.25
6.16	10.7	95.9	3.25
6.16	10.7	89.8	2.25
8.71	5.4	58.7	1.5
8.71	5.4	54.6	1.6
8.71	5.4	45.2	1.8
8.71	7.7	57.6	2.5
8.71	7.7	60.8	2.1
8.71	7.7	58.7	2.2
8.71	10.7	87.8	3.3
8.71	10.7	86.7	3.1

a_{max} and y_{max} are the maximum acceleration and penetration depth from the impact at speed V_i. Figure 7 presents normalized acceleration profiles from the tests. The majority of the waveforms exhibit characteristics of a plastic impact. Meyer's[10] theory provides a simplified description of plastic impacts in which the ground is assumed to exert a constant pressure on the impactor. This theory predicts maximum acceleration varies linearly with $V_i\sqrt{D/m}$ when penetrations are small relative to the diameter, D, of the penetrometer. Figure 8 compares the measurements for maximum acceleration as a function of this quantity. The full scale vehicle, with a nose radius of 0.66 m, impact speed of 30 m/s and mass of 26.3 kg, impacts at higher energies than achieved during the tests. The figure includes linear extrapolations to the expected value of 4.75 (MKS units) for the full scale vehicle impact and reveals the maximum expected acceleration during impact for the design in Fig. 4 is between 220 and 385 g's. Figure 9 plots penetration depth versus $V_i\sqrt{m/D}$ (also a relationship predicted by Meyer's theory). Extrapolation to the expected value of 189 (MKS units) reveals that the capsule in Fig. 4 should penetrate between 0.15 and 0.31 m. The variability in ground hardness at the three locations examined is responsible for much of the scatter in Figs. 7-9. In addition, the assumption of small penetration depths in Meyers theory which allows the linear extrapolations in Figs. 8 and 9 is not valid for some of the impacts. However, including the additional terms in the theory to remove this assumption would result in extrapolations in Fig. 8 which predict lower maximum accelerations.

Structural Design

The design in Fig. 4 contains two structural elements: the primary spherical structure and the structure required to support the conical frustum of the heatshield. For the purposes of this feasibility study, emphasis is placed on determining the required mass of each structure. The design of the primary spherical structure is discussed first.

The requirement for a stiff structure, whose deformation is limited during impact from a large range of possible attitudes, led to the decision to utilize a spherical structure of composite sandwich construction. Ground characterization tests at UTTR reveal that this structure must be sufficiently strong to undergo limited deformation during a 385 g impact. The structure will receive some cushioning from the heatshield material and foundation support from the energy absorbing material. To estimate the heatshield contribution, crush tests were performed on samples of PICA-15 as shown in Fig. 10. These measurements are used in the following finite-element analysis.

The primary spherical structure shown in Fig. 4 is a stiffness-based composite sandwich structure. Its 0.001 m thick face sheets are 2-D triaxial braid textile of intermediate modulus graphite fiber in a polyimide-class resin. The core is 0.0127 m of 40 kg/m^3 carbon foam. The total mass of the structure is 4.23 kg.

Dynamic finite element analysis provides the best available analytic tool for sizing this structure but requires detailed information on the mechanical properties and failure modes of each of the elements. To populate this set of empirical constants, a series of dynamic tests were performed on 0.3 m diameter graphite-epoxy hemispherical shells and sandwich structures. Figure 11 compares the crush response of 0.001 m graphite-epoxy shells under static and dynamic tests. The complete design of the structure using dynamic finite element analysis was incomplete at the time of writing of this paper. A simpler method

to illustrate the adequacy of this structure for the purposes of this feasibility study involves static finite element analysis.

From the UTTR ground characterization tests, an estimate of the acceleration profile of the capsule was determined. By assuming the entire mass of capsule must be decelerated according to this profile, a maximum expected static load on the structure and heatshield combination can be estimated. A static finite element analysis using MCS/NASTRAN[11] was performed. The model included the sandwich structure and the heatshield, but did not include the energy absorbing material which will act to increase the shell's stiffness. Figure 12 presents the maximum compressive strain predicted in the structure as a function of the applied load (in terms of $g's$). One design criteria used for this material specifies the compressive failure allowable at 450 K to be 0.0052. The structure should not fail unless accelerations in excess of 400 g's occur. The maximum strains occur around the impact point and decay rapidly away from that point. It is possible to take advantage of this distribution to tailor the strength of the spherical structure to reduce weight and move the c.g. position further forward. In addition, some localized failure of the structure at the impact point provides another mode for energy absorption and would be allowed as long as it doesn't greatly decrease the canister's crush stroke. For these reasons, the 4.23 kg allotted to the primary structure in the present design is judged adequate.

The secondary structure which supports the forebody heatshield beyond the spherical structure represents a traditional structural design. The requirement on this structure is that its deformations under aerodynamic deceleration loads are limited to values which will not risk fracture of the heatshield. This "wing" structure need not survive the ground impact. Ideally, at impact it would shear off decreasing the mass which the primary structure must decelerate. It is also available to provide some energy absorption during large-attitude or high-wind impacts. The design is a variation on a sandwich structure with the outer face sheet of 0.001 m graphite polyimide just behind the heatshield. The void between this face sheet and the spherical structure is filled with carbon foam of density 40 kg/m^3. The mass of the entire structure is 3.2 kg.

A prediction of the forebody pressure distribution at the maximum pressure point in the trajectory is shown in Fig. 13 where s is the distance along the surface from the geometric stagnation point. (This CFD prediction is discussed in the *Aerothermodynamics* section.) The compressive loads on this portion of the structure are around 3 psi. which are considerably less than the compressive strength of the foam as shown in Fig. 5. It appears possible to reduce the mass of this structure by using a thinner face sheet and decreasing the density of the foam.

Aerodynamics

Aerodynamic drag and stability of the design in Fig. 4 are required in hypersonic, supersonic, transonic, and subsonic flight regimes. The selection of the 45 degree half-angle cone aeroshell was the result of a trade among hypersonic drag (heating), subsonic drag (impact velocity) and subsonic stability (available crush stroke).

Figure 14 presents an approximation of the drag coefficient across the Mach range for the 45-degree half-angle shape. The hypersonic value, 1.04, was computed at Mach 31.7 and 21.2 using the Langley Aerothermodynamic Upwind Relaxation Algorithm (LAURA)[12]. (These solutions are described in detail in the *Aerothermodynamics* section.) The subsonic value, 0.68, comes from tests conducted in the Langley 20-foot Vertical wind tunnel[9] mentioned below. The supersonic and transonic values are from Brooks[13] and Nichols[14] wind tunnel data on a similar geometry. For the purposes of this feasibility study, the important values are the hypersonic value which affects the heat pulse and the subsonic value which determines the impact velocity.

Aerodynamic stability is a function of aeroshell shape and mass properties. A solid model of the design shown in Fig. 4 predicts the c.g. to be 0.314 m back from the nose. The spin-axis inertia is 2.23 $kg - m^2$. The pitch and yaw inertias are 1.60 and 1.53 $kg - m^2$ respectively. Aerodynamic stability is comprised of a static and dynamic component. For static stability, the slope of the moment curve at this c.g. location, $C_{m,\alpha}$, must be negative at the trim angle of attack (0^0 for this design). Figure 15 presents the variation in this parameter with Mach number. Static stability is highest in the hypersonic region (large negative $C_{m,\alpha}$). Static stability decreases near Mach 3 as the sonic line jumps from the nose to the shoulder of the vehicle.

In addition to the decrease in static stability indicated by $C_{m,\alpha}$, dynamic stability decreases at lower speeds and can become unstable in the transonic and subsonic flight regimes. If a vehicle is stable in the low subsonic speed regime, it will typically be stable at higher speeds. To examine the dynamic stability of blunt aeroshells considered for this design, a set of six mass-scaled spin-tunnel models were constructed. Figure 16 presents one attitude time history for a model geometrically similar to that shown in Fig. 4. The figure captures a test period immediately following a 35-degree intentional perturbation on the model and reveals the oscillations are decaying. The model is stable and the oscillations diminish to a limit cycle amplitude of less than 10 degrees. Moving the model's c.g. location further from its nose results in increased limit cycle amplitude and decreased amplitude of survivable perturbations. If the c.g. in the present design

were at 0.33 m back from the nose, the capsule could tumble in the subsonic portion of flight as a result of small perturbations. In addition to providing qualitative information on stability, the data in Fig. 16 is being analyzed to extract the static and dynamic aerodynamic characteristics of the shape.

Entry Trajectory and Landing Footprint

The geometry of the Earth approach trajectory is uncertain at this time. For this study, the exoatmospheric trajectory is assumed to have a V_∞ of 2.95 km/s, declination of -48.1 degrees, and right ascension of 284.9 degrees. This approach geometry results in North Polar (Azimuth 180 degrees) atmospheric entry with an inertial velocity of 11.46 km/s at 125 km altitude.

Figure 17 presents the velocity and altitude time history associated with entry of the 26.3 kg vehicle in Fig. 4 for an inertial flight path angle of -12 degrees. This entry angle was selected as the result of a trade between heatshield mass and aerodynamic deceleration. The maximum acceleration of 55.5 g's occurs at an altitude of 52.9 km, 39 seconds after the 125 km altitude atmospheric interface. Peak heating occurs at 33 seconds and 62.13 km altitude. After 91 seconds, the capsule has decelerated to Mach 1 and descended to 32.7 km altitude. The capsule attains terminal velocity shortly thereafter and impacts the ground (altitude = 1.3 km) at t = 541 seconds at a flight path of -90 degrees (vertical) while traveling 30 m/s.

An estimate of the landing footprint can be produced by varying mass, flight path angle, atmospheric properties and aerodynamic drag. The mass was varied plus or minus 1.25 kg (3-σ) around a nominal 26.3 kg value. Flight path angle was varied plus or minus 0.07 degrees. The Global Reference Atmospheric Model - 1995 (GRAM-95) was used to obtain variations in density, pressure and winds. Aerodynamic drag was varied plus or minus 5 percent in the hypersonic and subsonic regimes and 10 percent in the supersonic and transonic regimes. The resulting footprint for a 2500 case Monte-Carlo simulation overlayed on latitude and longitude of a UTTR landing site is shown in Fig. 18. The 3-σ landing ellipse is 40 km down range by 20 km cross range. Steepening the flight path angle or increasing the entry velocity will decrease the footprint dimensions while shallowing the flight path angle, decreasing velocity, or entering with a more Easterly azimuth will increase its dimension.

Aerothermodynamics, Heatshield, and Thermal Analysis

An estimate of the stagnation-point, non-ablating heating associated with the entry trajectory is shown in Fig. 19 (entry mass is 26.3 kg). The convective heating estimate comes from Chapman's equation and the radiative heating comes from the method of Tauber and Sutton[15]. The CFD predictions for convective heating are discussed below. Peak heating is predicted to be 580 W/cm^2 by the engineering approximations of which 534 W/cm^2 is convective. The stagnation point heat load is 9013 J/cm^2 from convective plus 265 W/cm^2 radiative for a total of 9277 J/cm^2.

The maximum heating point (t=33 s) and the maximum deceleration point (t = 39 s) in the heat pulse were computed using the LAURA CFD code[12]. An 11 species, thermochemical nonequilibrium gas-kinetic model with fully catalytic, radiative equilibrium wall boundary condition was used. The axisymmetric computational grid has 40 points along the body and 64 points normal to the surface with the first grid cell having a cell Reynolds number of 2. The non-ablating stagnation point heating predicted at the maximum heating and pressure points in the trajectory are shown as the circle symbols in Fig. 19, and the prediction for the entire forebody (assumed laminar) is shown in Fig. 20. The CFD prediction is 6 percent higher than the engineering estimate at peak heating and 1.6 percent higher at maximum pressure.

The flight Reynolds numbers based on diameter for these two cases are 150,500 and 299,000. (The peak Reynolds number during the heat pulse is 371,400 at a point where the heating has dropped to 13 percent of its peak value.) One indicator of the potential for transition to turbulence is the momentum thickness Reynolds number, Re_θ. Figure 21 presents values for the momentum thickness Reynolds number extracted from the two CFD solutions. A criteria for transition commonly used is 250. The figure indicates the Reynolds number effects may induce transition on the conical flank late in the heat pulse. Surface roughness and ablation out-gassing can also produce transition. A CFD solution using the Baldwin-Lomax turbulence model was generated at the maximum pressure location in the trajectory. The transition location was specified as the juncture between the spherical nose and conical frustum location (s = 0.25 m). That solution predicted convective heating on the flank of the body (which typically is a factor of 2.2 lower than the stagnation point value) to increase by a factor of 3.2 which results in flank heating 41 percent higher than the stagnation point value. If transition does not occur until peak heating, the integrated heat load to the flank of the vehicle and the required heatshield thickness is still less than the stagnation point. The question of transition must be examined closer. For the purposes of this study, a constant heatshield thickness sized for the laminar stagnation point heating environment is used over the entire forebody.

Phenolic Impregnated Carbon Ablator (PICA-15) is chosen as the candidate heatshield material. It is a lightweight ablator with density of 240 kg/m^3. To determine the required thickness, the estimate for to-

tal heating in Fig. 19 is increased by 20 percent (peak becomes 696 W/cm^2 and heat load becomes 11,132 J/cm^2). The thickness required is also a function of maximum allowable temperature in the underlying structure. Aluminum structures have specified 520 K as the maximum allowable temperature. The graphite polyimide structure has multiple use temperature limits of 540 K and single use limit of 643 K. Figure 22 presents the relationship between heatshield thickness and maximum bond line temperature predicted by the FIAT[16] material response code for this heat pulse. To limit bond line temperatures behind the heatshield to 520 K, the required heatshield thickness for these conditions is 0.0356 m (1.4 in.). To limit bond line temperatures to 650 K requires only 0.0229 m (0.9 in) of heatshield. The design in Fig. 4 provides 0.0381 m (1.5 in.) of PICA 15 so includes not only the 14-20 percent margin on heating but generous margins on thickness. This large margin will decrease if entry velocity increases.

The afterbody thermal protection system has not been examined in detail. The maximum heating on the afterbody is typically less than 5 percent of the forebody (results in an estimate of peak at 35 W/cm^2 and heat load of 550 J/cm^2). Large margins (factor of 3) are typically placed on afterbody heating predictions. A material such as SLA-561V (density 264 kg/m^3) as used on the afterbody of the Stardust Sample Return Capsule[2] may be an appropriate material. For mass purposes, 0.45 in of SLA561V covers the entire afterbody in the design shown in Fig. 4. This thickness is greater than that used on the Stardust afterbody which was designed for a more severe heating environment. The afterbody also contains penetrations for the attachment hard points, the electrical connection, and the lid. The environment at each of these penetrations will be less severe than those expected on similar penetrations on the Stardust afterbody. Seals and vents designed for that mission should be adequate here.

The temperature of the sample-containing canister must not exceed 370 K. A pre-impact thermal analysis was performed assuming the PICA-15 heatshield was 1.4 in. thick. The predicted temperature distribution at $t = 541$ s (impact) is shown in Fig. 23. The thermal energy is just beginning to penetrate into the energy absorbing material. At impact, however, the canister crushes into the heated material. A simple energy balance which assumes the 2.7 kg canister is all aluminum and that all of the thermal energy within 1 diameter of the canister ends up in the canister predicts the temperature rise in the canister to be 39^0 K. If the analysis is repeated to include all thermal energy within two diameters, the temperature rise is 94^0 K. This conservative energy balance approach did not include thermal losses to the air or the ground. During ground characterization tests, the ground temperature was measured to be 288 K.

Mission Scenario and Impact Performance

From launch through separation at Earth return, the capsule is attached to the MSR Orbiter via three attachment hard points on the afterbody of the primary spherical structure. The samples are contained in a hermetically sealed, biologically clean, canister which is transferred into the capsule on Mars orbit. This transfer and placement of the afterbody lid is accomplished via orbiter mechanisms.

During Earth return cruise, the canister seal integrity is monitored by orbiter electronics through an electrical connection on the capsule afterbody. Upon Earth arrival the entire bus is spun up to 5 rpm and positioned such that after separation (18 hrs prior to entry) the capsule enters at an inertial flight path angle of -12 degrees. Prior to separation, the ground recovery beacons are activated. (Each of the 2 beacons is assumed to be 0.3 kg which includes the 0.05 kg batteries necessary to supply each transmitter with 0.5 W of power for 24 hours.) The bus performs a deflection maneuver after separation. The attachment hard point locations act as vents during entry.

Ground impact (altitude 1295 m) occurs at 541 seconds after atmospheric interface. The impact velocity for zero surface winds is 30 m/s. If the impacted ground is similar to the ground examined at UTTR, the capsule will penetrate to a depth between 0.15 and 0.31 m in approximately 0.02 s. Of that time approximately 0.013 s is spent above 200 g's which will initiate crush of the canister into the energy absorbing material. There are several ways to estimate the distance the canister will crush into the 0.3 m of available energy absorbing material. The most conservative estimate neglects the energy absorbing contributions from the ground and the heatshield and predicts 0.23 m of required crush stroke. An estimate including the ground's contribution can be made by assuming the canister need decelerate only during the 0.013 s the loads on the capsule exceed 200 g's. This assumption decreases the predicted stroke to 0.17 m. If surface winds are a sustained 25 MPH (11.2 m/s), the resultant velocity is 32 m/s and an impact angle of incidence of 20.5 degs will occur. In this orientation, the available stroke is 0.29 m of which 0.26 m is necessary from the most conservative estimate. The landing footprint is a 40 by 20 km ellipse.

Mass Summary and Margins

A breakdown of the mass of each element of the design is provided in Table 2. No mass allotment has been included for the lid latches, the attachment hard points, or the canister-monitoring wiring. As with any design, there exists the semantic problem of specifying margins in terms of safety, mass, or a combination of both. The preceding sections discussed margins in terms of safety. In the absence of defined requirements

for those margins it is difficult to quantify that portion of the safety margin which could be redefined as mass margin for the elements in Table 2.

Table 2. Mass of each element of the suggested design in Fig. 4.

Element	Mass, kg
Heatshield and aft TPS	12.10
Heatshield Adhesive	1.40
Primary Structure	4.23
Wing Structure	3.19
Energy Absorbing Mat.	2.04
Canister	2.70
Beacons	0.60
TOTAL	26.26

Conclusion

A combination of analysis and testing was performed to determine the feasibility of an entirely passive Earth entry capsule for the Mars Sample Return mission. The design circumvents the potential failure modes of a parachute terminal descent system by replacing that system with passive energy absorbing material to cushion the Mars samples during ground impact. The suggested design utilizes a spherically blunted 45 degree half-angle forebody with a low-density, ablative heatshield. The primary structure is a spherical composite sandwich enclosing carbon foam energy absorbing material. Results of the testing and analysis presented indicate that the design is an option worthy of further study for the Mars Sample Return Mission.

Acknowledgments

Thanks are extended to Mark Adler of the Jet Propulsion Laboratory for supporting this work. Dr. Y. K. Chen and Huy Tran of NASA ARC provided the heatshield sizing and pre-impact thermal analysis. Mr. David Mitcheltree and Capt. James Theiss assisted in the UTTR ground characterization tests. Nelson Seabolt constructed much of the impact test hardware including the ground penetrometers. Matt Hendrickson performed the solid modeling of the design. Mike Fremaux conducted the vertical spin tunnel tests. Ed Fasanella assisted in the structural design.

References

[1]Hermann, R. J. and Lineberger, W. C. "Mars Sample Return: Issues and Recommendations," Task Group on Issues in Sample Return, Space Studies Board, National Research Council, ISBN 0-309-057337, National Academy of Sciences, 1997.

[2]Atkins, K. L. Brownlee, D. E. Duxbury, T. Yen, C. and Tsou, P. "STARDUST: Discovery's Interstellar Dust and Cometary Sample Return Mission," Proceedings from the 1997 IEEE Aerospace Conference, Feb., 1997.

[3]Mitcheltree, R. A. Wilmoth, R. G. Cheatwood, F. M. Brauckmann, G. J. and Greene, F. A. "Aerodynamics of Stardust Sample Return Capsule," AIAA 97-2304, June, 1997.

[4]Williams, S. D. "A Preliminary TPS Design for MRSR - Aerobraking at Mars and at Earth," AIAA 90-0052, Jan., 1990.

[5]Meyerson, R. E. and Cerimele, C. J. "Aeroassist Vehicle Requirements for a Mars Rover/Sample Return Mission," AIAA Paper 88-0303, Jan., 1988.

[6]Gamble, J. D. "JSC Pre-Phase-A Study Mars Rover Sample Return Mission Aerocapture, Entry, and Landing Element," JSC-23230, May, 1989.

[7] Brauer, G. L. Cornick, D. E. and Stevenson, R. "Capabilities and Applications of the Program to Optimize Simulated Trajectories (POST)," NASA CR-2770, Feb. 1977.

[8] Hoerner, S. F. *Fluid-Dynamic Drag*, Published by the Author, 1965.

[9]Neihouse, A. I. Kliner, W. J. and Scher, S. H. "Status of Spin Research for Recent Airplane Designs," NASA TR R-57, 1960.

[10]Goldsmith, W. *Impact*, Edwin Arnold Ltd., London, 1960.

[11] Lahey, R. S. Miller, M. P. and Reymond, M., "MSC/NASTRAN Reference Manual Version 68," The MacNeal Schwendler Corporation, 1994.

[12]Cheatwood, F. M. Gnoffo, P. A. "User's Manual for the Langley Aerothermodynamic Upwind Relaxation Algorithm (LAURA)," NASA TM-4674, Apr., 1996.

[13]Brooks, J. D. "Some Anomalies Observed in Wind Tunnel Tests of a Blunt Body at Transonic and Supersonic Speeds," NASA TN D-8237, June, 1976.

[14]Nichols,
J. O. and Nierengarten, E. A. "Aerodynamics Characteristics of Blunted Bodies," JPL TR 32-677, 1964.

[15]Tauber, M. E. and Sutton, K. "Stagnation Point Radiative Heating Relations for Earth and Mars," *Journal of Spacecraft and Rockets*, Vol 28., No. 1, Jan.-Feb., 1991, pp. 40-42.

[16]Chen, Y. K. and Milos, F. S. "Fully Implicit Ablation and Thermal Analysis Program (FIAT)," Presented at the Fourth International Conference on Composites and Engineering, Kona, HI, July, 1997.

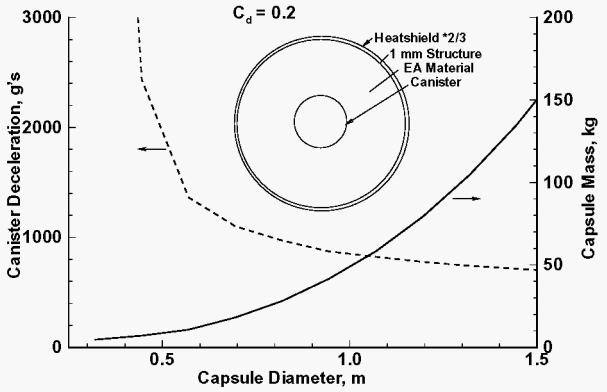

Fig. 1 Canister loads and impact velocity of omnidirectional spherical capsule.

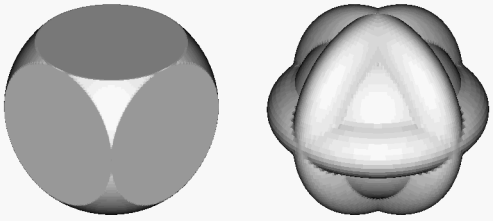

Fig. 2 Modified spherical omnidirectional concepts to increase subsonic drag.

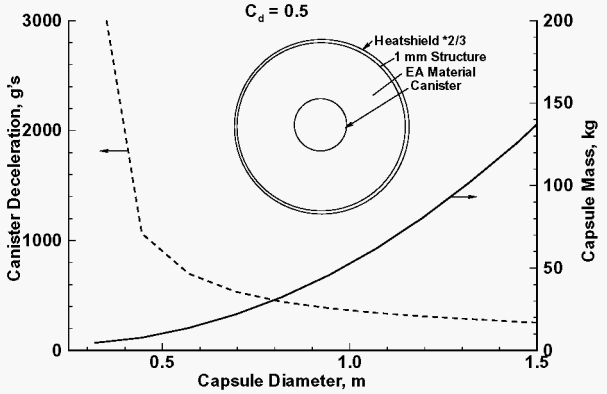

Fig. 3 Canister loads and impact velocity of modified spherical concepts (C_D = 0.5).

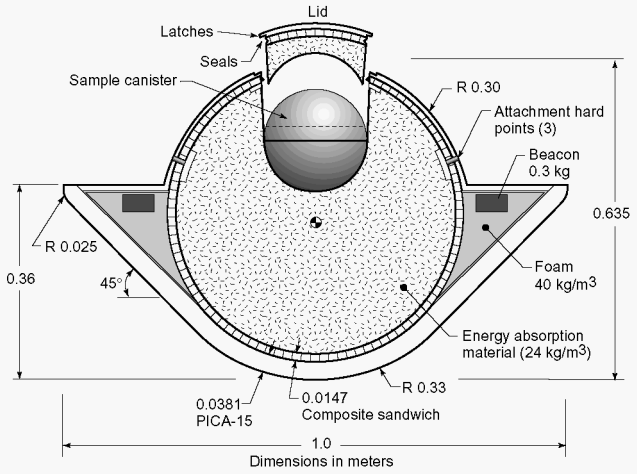

Fig. 4 Hybrid directional design schematic

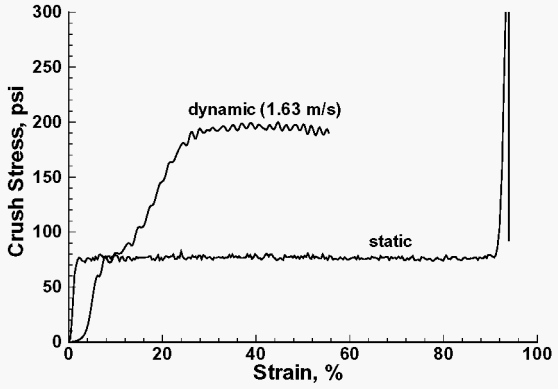

Fig. 5 Static and dynamic crushing strength of 60 kg/m^3 carbon foam

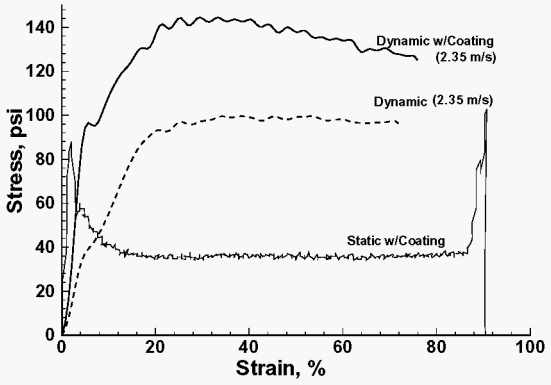

Fig. 6 Effect of surface coating on static and dynamic crushing strength of 51 kg/m^3 carbon foam

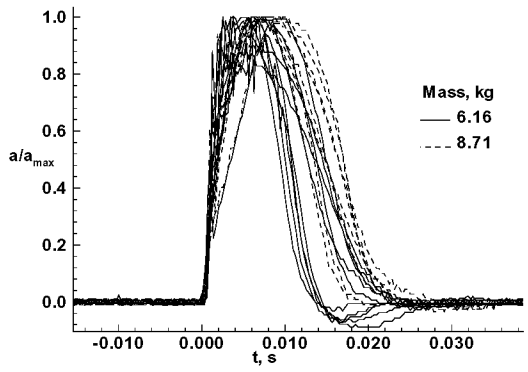

Fig. 7 Normalized acceleration waveforms measured at UTTR impact tests

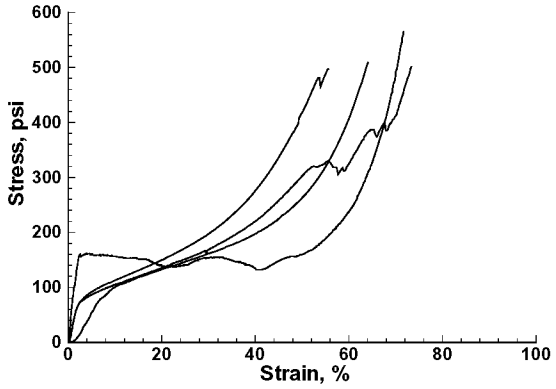

Fig. 10 Static crush strengths of 4 samples of PICA-15 taken from an arc-jet tested model

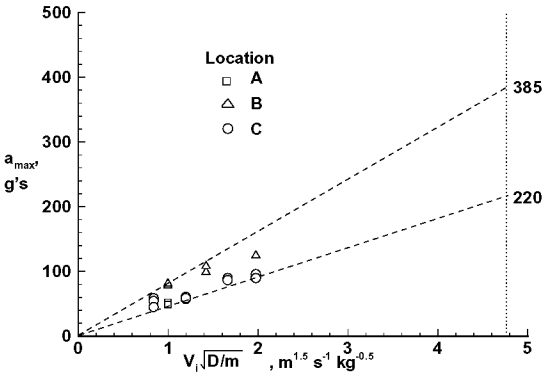

Fig. 8 Variation in maximum acceleration from UTTR impact tests

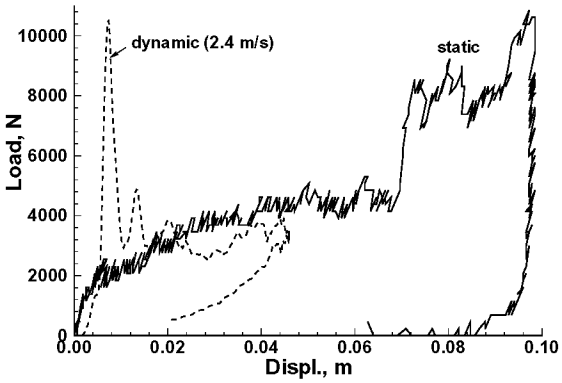

Fig. 11 Static and dynamic crush of 0.001 m thick, 0.3 m diameter, graphite-epoxy shells

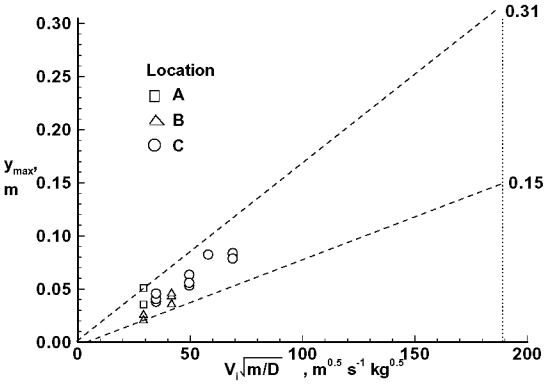

Fig. 9 Variation in penetration depth from UTTR impact tests

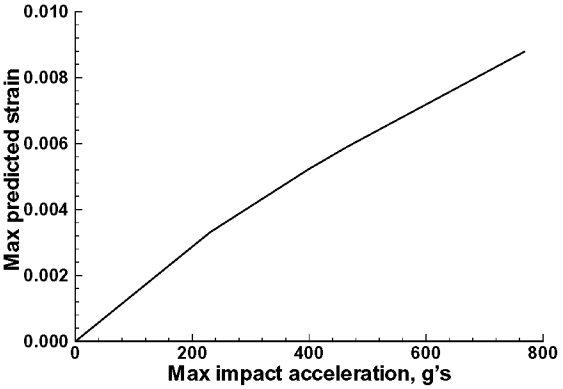

Fig. 12 Maximum predicted compressive strain in the primary spherical structure for different static loads placed on the heatshield/structure combination

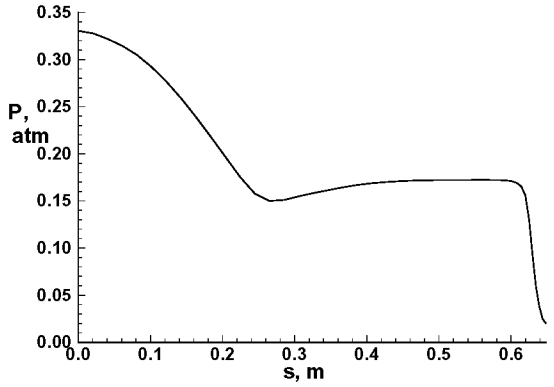

Fig. 13 Maximum forebody pressures at Mach 22.8 for 45 degree half-angle design

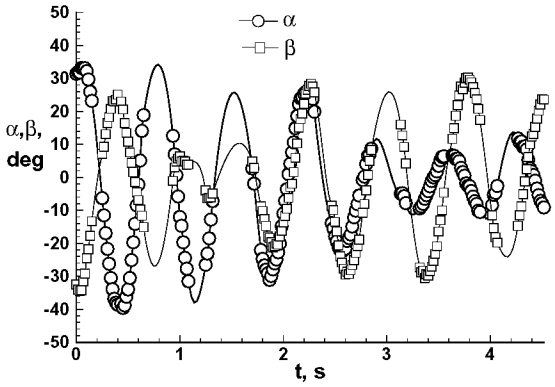

Fig. 16 Decay of large perturbation on 0.356 scale model of 45 deg cone in 20-Foot Vertical Spin Tunnel

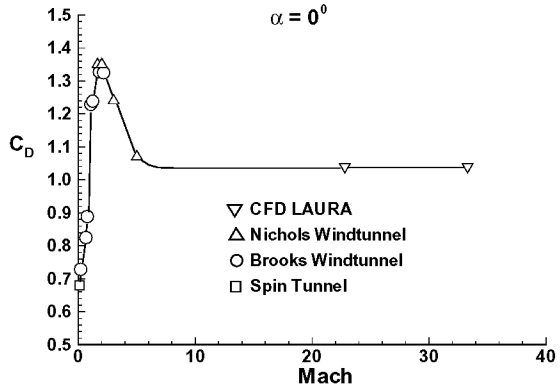

Fig. 14 Drag coefficient variation with Mach number for 45 degree half-angle design

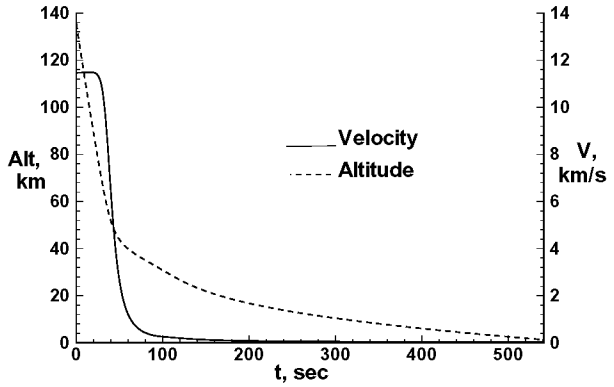

Fig. 17 Entry trajectory speed and altitude for -12 degree entry angle

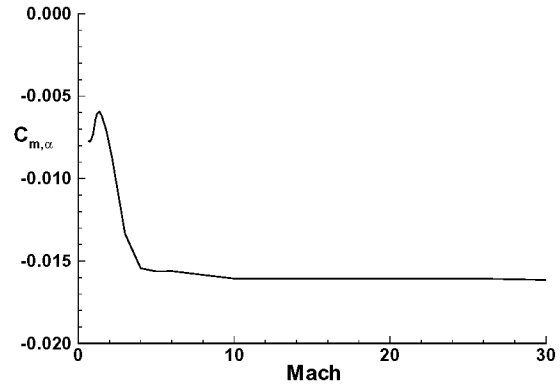

Fig. 15 Moment coefficient slope variation with Mach number for 45 degree half-angle design

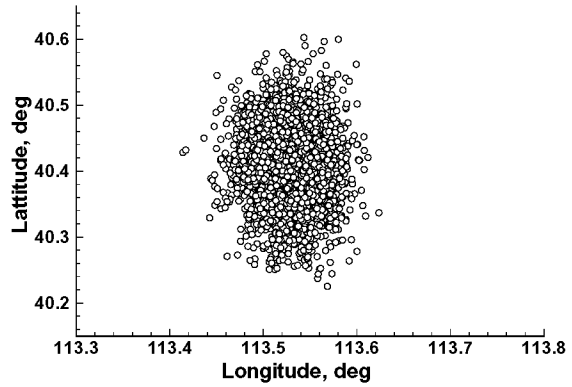

Fig. 18 Landing footprint from dispersion on initial entry vector, entry mass, atmosphere, and drag

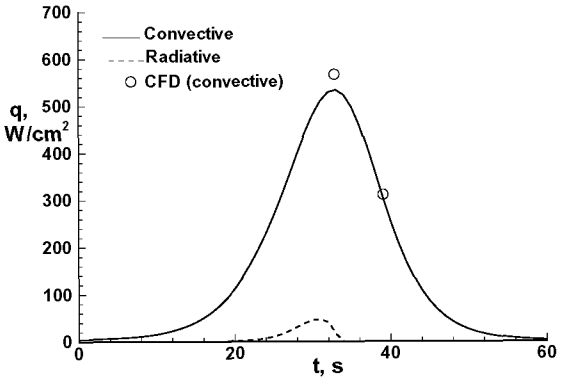

Fig. 19 Chapman's equation estimate of convective heating and Tauber-Sutton estimate of radiative heating at the stagnation point

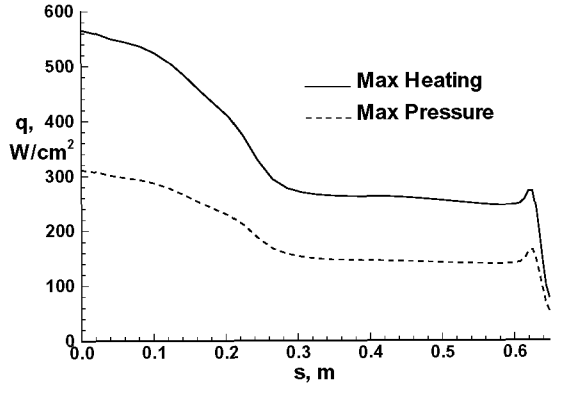

Fig. 20 Nonablating, laminar, forebody heating at maximum heating and pressure trajectory points from LAURA CFD.

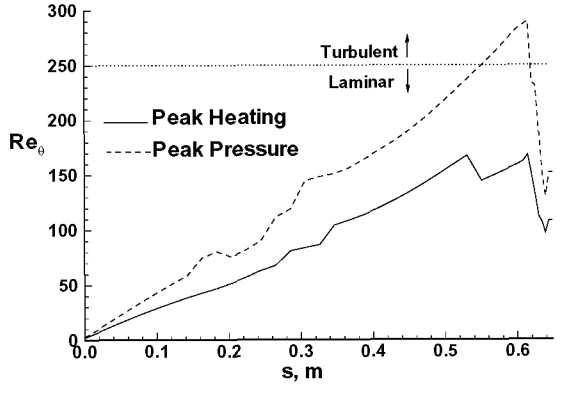

Fig. 21 Momentum thickness Reynolds numbers extracted from maximum heating and pressure CFD solutions.

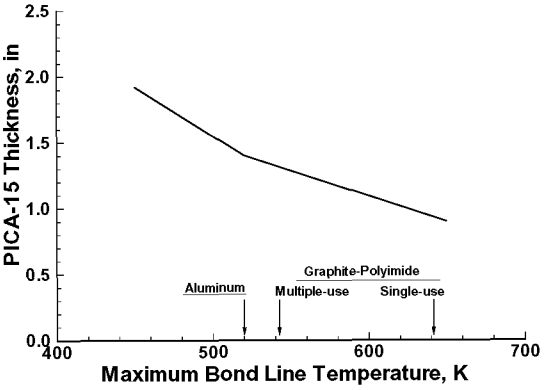

Fig. 22 Relationship between heatshield thickness and maximum temperature experienced by the underlying structure.

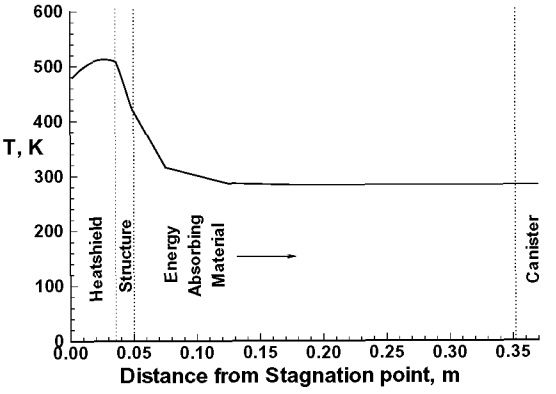

Fig. 23 Temperature distribution across heatshield, structure, and energy absorbing material at time of ground impact.